

Invasion percolation with viscous forces

B. Xu and Y. C. Yortsos*

*Petroleum Engineering Program, Department of Chemical Engineering, University of Southern California,
Los Angeles, California 90089-1211*

D. Salin

Laboratoire Fluides, Automatique et Systèmes Thermiques, Batiment 502, Campus Universitaire, 91405 Orsay Cedex, France

(Received 20 February 1996; revised manuscript received 30 June 1997)

We study invasion percolation in the presence of viscous forces, as a model of the drainage of a wetting fluid from a porous medium. Using concepts from gradient percolation, we consider two different cases, depending on the magnitude of the mobility ratio M . When M is sufficiently small, the displacement can be modeled by a form of gradient percolation in a *stabilizing* gradient, involving a particular percolation probability profile. We develop the scaling of the front width and the saturation profile, in terms of the capillary number. In the opposite case, the displacement is described by gradient percolation in a *destabilizing* gradient and leads to capillary-viscous fingering. This regime is identified in the context of viscous displacements and in general differs from diffusion-limited aggregation, which also describes displacements at large M . Constraints for the validity of the two regimes are developed. Limited experimental and numerical results support the theory of stabilized displacement. The effect of heterogeneity is also discussed. [S1063-651X(97)08812-0]

PACS number(s): 47.55.Mh, 0.5.40.+j, 47.55.Kf

I. INTRODUCTION

The displacement (drainage) of a wetting fluid (subscript w) in a porous medium by the injection of another nonwetting fluid (subscript nw), immiscible to the former, has been analyzed in great detail in past studies. In the absence of viscous or gravity forces, slow drainage is controlled solely by the capillary pressure $P_c = P_{nw} - P_w$ (the difference in pressure between the two fluids), which is spatially uniform. At the pore-network level, this problem can be modeled by invasion percolation (IP), in which the front separating the two fluids advances by penetrating the pore throat at the front with the largest size (smallest capillary resistance). The properties of IP and its close connection to ordinary percolation (OP) have been extensively studied [1–4].

In the presence of gravity [5–7], or of a gradient in the average pore size (permeability) [8], and in the absence of viscous forces, slow drainage has been modeled with invasion percolation in a gradient (IPG), which is a modified version of gradient percolation (GP). Here the capillary pressure varies linearly (or almost linearly) in the direction of displacement x . Because of their direct relationship (see below), this gradient also results in a gradient in the percolation probability p , usually expressed in terms of the bond number B (where $B \sim -dp/dx$). For example, in invasion in a hydrostatic gradient, $B = \Delta\rho g_x r_m^2 / \gamma$, where $\Delta\rho$ is the density difference, g_x is the gravity component in the direction of displacement, r_m is a typical throat size, and γ is the interfacial tension between the two fluids. For invasion in a permeability gradient, $B = -dk^{1/2}/dx$, where k is the permeability [8]. In IP ($B=0$), the entire displacement pattern is a percolation cluster. However, in IPG, one needs to distin-

guish two different cases, depending on whether percolation is in a stabilizing or a destabilizing gradient.

In the first case ($B>0$), for example in the downward displacement at capillary control of a heavier fluid by the injection of a lighter fluid or in drainage in a field of decreasing permeability, the percolation probability decreases in the direction of displacement. The region where the invasion has the characteristics of a percolation cluster is only of a finite extent σ , which was shown in [5,6,9] to scale as

$$\sigma \sim B^{-\nu/(\nu+1)}, \quad (1)$$

where ν is the correlation length exponent of percolation [10,11]. Here σ denotes the width of the front (in two dimensions) or of the front tail (in three dimensions) (see [6] for the necessity for this distinction), where the displacing pattern has the structure of the percolation cluster and fractal concepts apply. Equivalently, σ measures the maximum extent of the correlation length, which in gradient percolation problems becomes finite due to the applied gradient. Various properties of GP and IPG have been studied in considerable detail [5,8,12–14]. In invasion in a destabilizing gradient ($B<0$), for example, in the downward displacement at capillary control of a lighter fluid by the injection of a heavier fluid or in drainage in a field of increasing permeability, the percolation probability increases in the direction of displacement. Then the displacement proceeds in the form of capillary fingers, the scaling of the average thickness of which with (the absolute value of) the Bond number also satisfies Eq. (1) [14–16].

In the presence of both viscous and capillary forces, the displacement is characterized by three dimensionless numbers: the capillary number $Ca = q\mu_{nw}/\gamma$, where q is the injection velocity and μ_{nw} the viscosity of the displacing phase; the viscosity ratio $M = \mu_w/\mu_{nw}$, where μ_w is the viscosity of the displaced phase; and the dimensionless system

*Author to whom correspondence should be addressed.

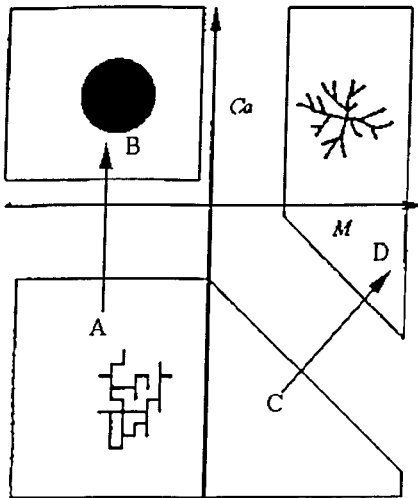


FIG. 1. Phase diagram for drainage (adapted from [17]). Arrows indicate the transition from percolation to viscous-dominated regions.

size L (expressed in units of the average pore length l). As Ca or L increases, the viscous pressure drop in the two fluids becomes comparable to capillarity and one expects that some form of gradient percolation would also describe this process. Work in this direction was reported in the following three studies.

Wilkinson [9] proposed concepts of GP for modeling viscous displacements. He assumed a stabilized displacement and developed a power-law scaling between the front extent and the capillary number, of the form $\sigma \sim Ca^{-a}$, where $a = \nu/(t - \beta + 1 + \nu)$ and t and β are the OP exponents scaling conductivity and percolation probability, respectively [10]. In a somewhat related study of the drainage of a wetting fluid in an $L \times L$ square lattice, Lenormand [17] delineated the limiting domains in parameter space (Ca, M, L), where fractal patterns (including percolation) apply. His phase diagram in (Ca, M) space, with the present convention for M , is shown schematically in Fig. 1. Lenormand found that a power law relates the domain boundaries to the system size and obtained the exponents $\nu/(t + 1 + \nu)$ and $\nu/(1 + \nu)$ for the percolation-to-compact and the percolation-to-viscous fingering boundaries, respectively. It will be shown below that Lenormand's work is essentially a study in GP (in both a stabilizing and a destabilizing gradient), even though his problem does not involve the propagation of a front or a saturation profile. Blunt, King, and Sher [18] provided arguments about the extent of the frontal region similar to Wilkinson's, but proposed the different exponent $\nu/(t - \nu + 1)$ for the scaling with the capillary number. Interestingly, all these exponents differ from one another, suggesting that a general consensus on this issue has not yet been reached.

The effect of viscous forces on displacements in porous media is of obvious importance to process scale-up and large-scale simulations. As length scales increase, viscous effects are increasingly dominant over capillarity. An understanding of this competition at the pore-network scale is necessary to provide insight into the validity of the conventional continuum description using relative permeabilities, which is standard practice in commercial simulations [19]. Although

conventionally used, the very concept of relative permeabilities still remains a subject of debate, particularly in connection to displacements in heterogeneous media [20] and viscous fingering. For example, it is known that under conditions of sufficiently large M and Ca , immiscible displacement becomes unstable (see, e.g., [21,22]) and in the large- M and $-Ca$ limit can be described by diffusion-limited aggregation (DLA) (see also Fig. 1). In this paper we attempt to provide some insight into these problems. We consider fully developed drainage in uncorrelated random media in the presence of viscous forces and proceed by postulating an analogy with IPG. Depending on the relative magnitude of M , we anticipate the existence of two different regimes, described by IPG in a *stabilizing* or a *destabilizing* gradient, respectively. These two regimes dictate the development of the saturation profiles in the respective displacements. In a related sense, they also characterize, under dynamic displacement conditions, the percolation-to-compact and percolation-to-DLA transitions described in Lenormand's [17] phase diagram (Fig. 1).

In the stabilized case, the saturation profiles approach a well-known traveling-wave state. As in standard GP, we anticipate the existence of a frontal region with the structure of a percolation cluster, but of a finite extent, here limited by viscous pressure gradients, where fractal behavior applies, followed by an upstream region with the characteristics of a compact pattern. This is the percolation-to-compact transition of Lenormand's phase diagram (arrow AB in Fig. 1). To describe the frontal region, we will propose an extension of IPG, based on viscous forces, from which the scaling of the front width with the capillary number can be derived. We show that the exponent obtained is identical to Wilkinson's [9], although the two approaches are conceptually different. In the destabilized case, IPG in a destabilizing gradient applies [15] and the displacement should proceed in the form of fingers, the size of which depends on the capillary-viscous competition, in analogy to the case of gravity-unstable capillary invasion. This is the percolation-to-viscous fingering transition of Lenormand's phase diagram (arrow CD in Fig. 1). We will show that under certain conditions, the exponent scaling the size of the fingers is identical to that obtained by Lenormand [17] for the size dependence of the percolation-to-DLA boundary. We comment on the conditions that delineate the validity of these scalings in the two different cases, which is described in more detail in [23]. As the stabilized displacement is also described in a continuum formulation by the Buckley-Leverett equation (see standard texts, and also [9,24]), the constraints developed are essentially those for the validity of the Buckley-Leverett formalism. The scaling theory is partially tested with numerical simulation using pore networks and with experiments conducted in model porous media. We conclude with some discussion of the effect of heterogeneity on the continuum description.

II. THEORY

We consider drainage in a rectilinear porous medium, which is conventionally represented as a random, spatially uncorrelated network of pores (e.g., a rectangular lattice of size $L \times N$ in two dimensions or a lattice of size $L \times L \times N$ in three dimensions, where N is variable). We take sufficiently

large L to suppress finite-size effects at the front, which are particularly important at low rates. We assume a constant lattice spacing l , a variable pore throat size distribution with probability density function $\alpha(r)$, mean r_m , and standard deviation Σr_m , where Σ is a dimensionless standard deviation, and we take sites of equal volume. The drainage of a fluid of viscosity μ_w by another fluid of viscosity μ_{nw} at the constant volumetric flow rate Q is considered. The fluids are incompressible, thus the total flow rate across any cross section is constant and equal to the injected Q . However, this rate is partitioned differently in the two different phases at different places, namely, $Q_w = F_w Q$ and $Q_{nw} = (1 - F_w)Q$, respectively, where the fractional flow term F_w is a function of distance and also must be determined.

In the absence of viscous forces, the capillary pressure is spatially uniform and the displacement proceeds by following the usual rules of IP, namely, by successively invading the perimeter pore with the largest size. In the presence of a viscous pressure drop, a gradient in the capillary pressure (negative or positive) is generally expected to develop. In view of the relations

$$P_c = \frac{2\gamma}{r} \quad (2)$$

and

$$p = \int_r^\infty \alpha(r) dr \quad (3)$$

[more correctly $p = \int_{r_{\min}}^\infty \alpha(r) dr$, where r_{\min} is the minimum throat size invaded], this in turn implies a gradient in the percolation probability. Problems involving a constant gradient in p are amenable to GP and IPG, thus we expect that a similar description would also be applicable in the present case involving viscous forces. For example, Fig. 2 shows typical patterns of viscous displacements for $M=0.1$, obtained from pore-network simulation in the absence of trapping (details of the simulation can be found in [25,26]). When Ca is low [Fig. 2(a)], viscous forces are negligible and the pattern has the fractal structure of the IP cluster. As viscous forces increase at larger Ca [Figs. 2(b)–2(d)], however, the front takes the appearance of a rough (self-affine), rather than self-similar, curve and has an extent that decreases with increasing Ca . These trends are consistent with a gradient percolation description.

Following GP notions, we will distinguish two different cases: one in which the percolation probability p (hence P_c) decreases in the direction of displacement and that has features similar to GP in a stabilizing gradient and another in which p (hence P_c) increases in the direction of displacement, with features similar to GP in a destabilizing gradient. Because in our problem the capillary pressure P_c is controlled by the viscous pressure drop (rather than gravity, as in the case of buoyancy [9]), the viscosity ratio M is expected to be an important parameter in delineating these two regimes.

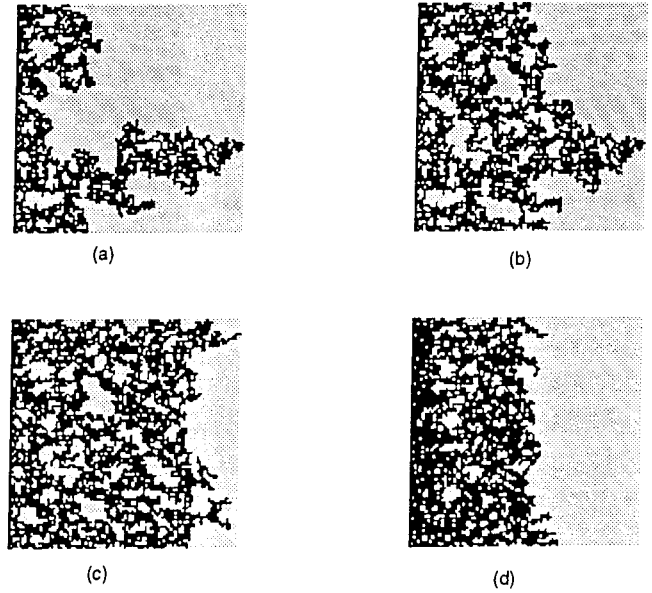


FIG. 2. Displacement patterns from numerical simulation of drainage in a 100×100 lattice, with $M=0.1$ and different values of the capillary number: (a) $Ca=3.2 \times 10^{-8}$ (IP), (b) $Ca=3.2 \times 10^{-6}$, (c) $Ca=3.2 \times 10^{-5}$, and (d) $Ca=3.2 \times 10^{-4}$.

A. Stabilized displacement

In the case of a stabilized displacement, we follow [6] and define the location $X_c(t)$, as the place where the transverse average of the percolation probability is equal to the percolation threshold p_c , namely,

$$p(X_c) = p_c. \quad (4)$$

In two-dimensional (2D) lattices, X_c represents the mean front position. The regions on either side of X_c of an extent σ (namely, between $X_c - \sigma$ and $X_c + \sigma$) have the fractal properties of the percolation cluster [6]. In 3D lattices, however, due to the higher connectivity, X_c does not represent the mean front position (here the front extends far upstream), but rather denotes a mean leading edge. Nonetheless, a percolation pattern is also expected around X_c . Following [6], we will focus on the front-tail region ($X > X_c$), the extent of which we will also denote by σ . As in the corresponding IPG problem, $X_c(t)$ varies linearly with time in either 2D or 3D geometries, with a velocity v , to be determined. In both cases, the fractal regions are followed by an upstream region (which also includes the ‘‘critical region’’ in the terminology of [9]), where both invading and invaded phases are compact [6] and the conventional continuum description is valid. A qualitative sketch of the two regions along with the notation used is shown in Fig. 3. These two regions will be analyzed separately. We note in advance that Wilkinson’s [9] analysis (using a continuum description) was based on the compact regime only, while Lenormand’s [17] is on the fractal regime (but only for a 2D geometry). For convenience, we will use the term ‘‘frontal region’’ to denote the region where fractal behavior applies in both 2D and 3D geometries and we will use σ to denote, in units of lattice spacing, its extent, namely, the front width or the front-tail width in the respective geometries. In this context, σ also represents the maximum

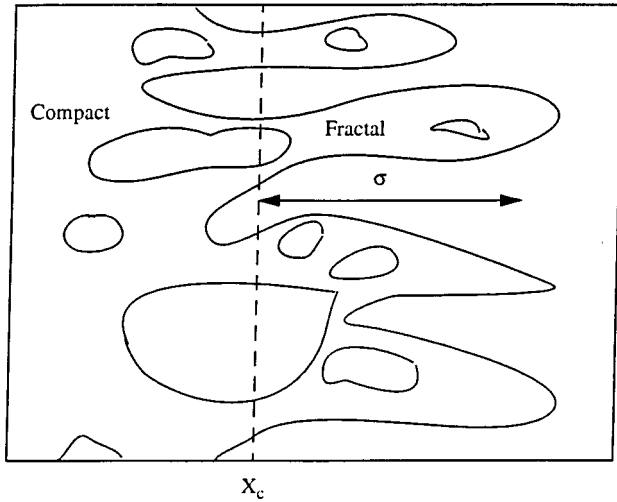


FIG. 3. 2D schematic of the 3D front region and the notation used.

extent of the correlation length, which in gradient percolation is “trapped” in a region of finite extent. Our emphasis will be on 3D problems to avoid unnecessary complications due to trapping issues associated with 2D displacements [27].

1. Frontal region

Consider the frontal region of width σ and lateral extent L^{d-1} , where d is the embedding dimension. We will focus on two main properties: the scaling of σ and the saturation profile. It is necessary that an estimate of the viscous pressure drops in the two phases be derived. Although straightforward when fluids occupy a compact pattern, the problem is more complex when they occupy a fractal pattern, as is the case with the nonwetting phase in this region.

To estimate the pressure drop of the nw phase ΔP_{nw} , we partition the region in equal size “boxes” of size σ^d and consider the pressure drop across such a box. This partitioning is necessary for the application of percolation scaling laws and was also used in [6] to estimate the number of sites on the front. Because the displacement pattern is part of a percolation cluster, the dimensionless conductance of the nonwetting phase in the box G_{nw} has the scaling [10]

$$G_{nw} \sim \sigma^{-\zeta/\nu}, \quad (5)$$

where ζ is the conductance exponent ($\zeta = 1.30$ or 1.12 in two or three dimensions, respectively [10,11]) and it was assumed that σ is sufficiently large for these scalings to be applicable. The exponent ζ is simply related to the conductivity exponent t used in the previous studies, $t = \zeta + (d - 2)\nu$ (the two coincide in 2D geometries). The volume flow rate of the nw phase across each box $Q_{i,nw}$ is determined from the overall volume flow rate Q_{nw} by a simple mass balance

$$Q_{i,nw} = \frac{Q_{nw} \sigma^{d-1}}{L^{d-1}}. \quad (6)$$

Combining Eqs. (5) and (6) gives the following estimate for the pressure drop of the nw phase across the frontal region:

$$\Delta P_{nw} = \frac{A Q_{nw} \mu_{nw}}{L^{d-1} r_m^3} \sigma^{\zeta/\nu + d - 1} \quad (7)$$

where A is a dimensionless constant of order 200 [5,28], we implicitly used a Poiseuille-type model for the conductance across a pore and we also assumed that the lattice spacing l is proportional to the average throat size r_m .

For further progress, an expression for Q_{nw} is required. We postulate that quantities at the front reach a steady state in a coordinate system moving with the front velocity v . The fact that stabilized immiscible displacements reach a traveling-wave state is well known and has been established theoretically (e.g., see [9,29]) and experimentally. Then a mass balance on the nw phase in the frontal region leads to

$$Q_{nw} = \phi v L^{d-1} l^2 S_{nw}, \quad (8)$$

where ϕ is porosity and the saturation S_{nw} is the transverse average of the fraction of sites occupied by the nw phase. Now, in the region under consideration, the displacing phase consists of a part of the percolation cluster, thus $S_{nw} \sim \sigma^{D-d}$, where D is the mass fractal dimension, and Eq. (8) becomes

$$Q_{nw} = B v L^{d-1} l^2 \sigma^{D-d}, \quad (9)$$

where B a dimensionless constant. At this point, we must emphasize the difference between this approach and Lenormand’s [17], where the entire rate Q was used in the calculation of the pressure drop (see also below). By contrast, Eq. (9) implies that only a fraction of Q actually reaches the frontal region, at least under conditions of a traveling state of constant velocity. This difference will be ultimately reflected in the scaling exponents to be derived.

Determining the magnitude of the velocity requires the solution of the overall problem, including the consideration of the region away from the front. This approach involves the solution of the Buckley-Leverett problem, discussed in various standard references (see also [8,22]). For the purposes of this section, however, we will only note the simple scaling result $v \sim Q/L^{d-1} l^2$, which to leading order is independent of the capillary number. Thus, using Eq. (9) we may express Eq. (7) as

$$\Delta P_{nw} = \frac{C v l^2 \mu_{nw}}{r_m^3} \sigma^{[\zeta + \nu(D-1)]/\nu}, \quad (10)$$

where $C = AB$. Equation (10) shows that because of the fractal nature of the displacing phase, the viscous pressure drop in the nw phase scales *nonlinearly* with its extent.

Estimating the pressure drop of the wetting phase is straightforward. The displaced phase is compact, hence we can use continuum theory. Making use of Eq. (6), with an obvious change in notation, and of the continuum scaling $G_w \sim \sigma^{d-2}$ and taking, to leading order in this region, the approximation $Q_w \approx Q$ gives the estimate

$$\Delta P_w = \frac{E q l \mu_w}{r_m^2} \sigma, \quad (11)$$

where the constant E is of the same order as C and we also introduced the mean flow velocity $q = Q/L^{d-1}l^2$. Combining Eqs. (10) and (11) gives the variation of P_c across the front

$$\Delta P_c = \Delta P_{nw} - \Delta P_w = \frac{Cv l^2 \mu_{nw}}{r_m^3} \sigma(\sigma^{[\xi + \nu(D-2)]/\nu} - bM), \quad (12)$$

where we introduced the $O(1)$ constant $b \equiv q r_m E / \nu l C$. We recall that the ratio q/ν is $O(1)$ and decreases with M , as dictated by the Buckley-Leverett solution. Note that for the stabilized displacements assumed in this section, the right-hand side of Eq. (12) must be positive, namely, $\sigma^{[\xi + \nu(D-2)]/\nu} - bM > 0$ (see below).

Consider next the variation in p . From Eqs. (2) and (3) we have

$$\Delta P_c \approx -\frac{2\gamma\Delta r}{r_m^2} \approx \frac{2\gamma\Sigma\Delta p_F}{r_m}, \quad (13)$$

where all increments express differences between upstream and downstream quantities and we used subscript F to denote the frontal region. The term Δr indicates the difference in the minimum size of pore throats penetrated by the non-wetting phase across this region. When $\Delta P_c > 0$, then $\Delta r < 0$, which means that progressively smaller throats are penetrated upstream (hence leading towards a more compact displacement) and vice versa. Combining Eq. (13) with Eq. (12), we find

$$\Delta p_F \approx \frac{Ca_F C l^2}{2\Sigma r_m^2} \sigma(\sigma^{[\xi + \nu(D-2)]/\nu} - bM), \quad (14)$$

where we introduced the modified capillary number $Ca_F \equiv \nu \mu_{nw} / \gamma$ based on the front velocity (see also [9]). Equation (14) shows that in contrast to standard GP and IPG, the change in the overall percolation probability in the viscous problem is *not* linearly related to the size of the overall increment. However, as will be shown below, the spatial probability profile across this region of extent σ is linear. We can obtain the scaling of the front width by applying the self-consistency argument of gradient percolation [6,9]. As σ delineates the extent over which percolation scalings apply, we also have

$$\Delta p_F \sim \sigma^{-1/\nu}, \quad (15)$$

which, combined with Eq. (14), yields the algebraic equation

$$\sigma^{1/\nu+1} (\sigma^{[\xi + \nu(D-2)]/\nu} - bM) \approx \frac{2\Sigma}{Ca_F C}, \quad (16)$$

where we absorbed into C a constant of $O(1)$. The solution of Eq. (16) provides the dependence of the front width σ as a function of Ca and M . For typical values in three dimensions, this equation reads

$$\sigma^{2.14} (\sigma^{1.77} - bM) \approx \frac{2\Sigma}{Ca_F C}, \quad (17)$$

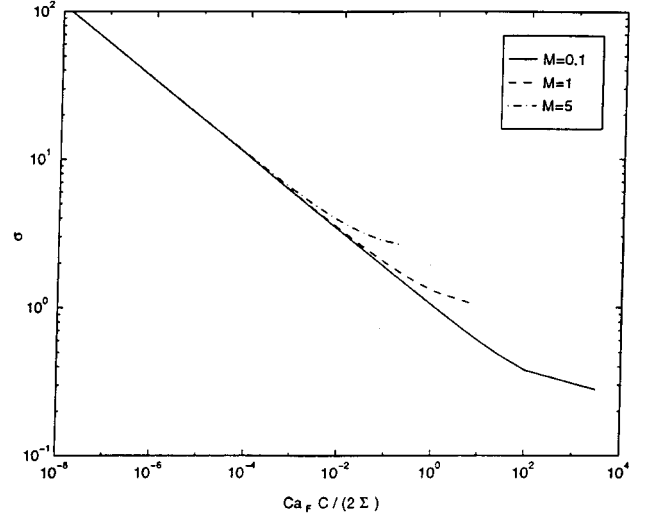


FIG. 4. Numerical solution of Eq. (16) vs modified capillary number for three different values of M .

It is important to note that Eq. (16) admits a unique solution for *all* values of M and Ca_F . This can be readily seen by rearranging the equation in the form

$$\sigma^{[\xi + \nu(D-2)]/\nu} - \frac{2\Sigma}{Ca_F C} \sigma^{-(1/\nu+1)} \approx bM \quad (18)$$

and noting that its left-hand side is a monotonically increasing function of σ . This has relevance to the development of constraints for the validity of stabilized displacement, as discussed below and in [23].

The solution of Eq. (16) increases with an increase in M and decreases with an increase in the front capillary number Ca_F . Figure 4 shows numerical results for typical parameter values in 3D geometries. The solution approaches a constant value at large Ca_F and a power-law asymptote at small Ca_F . Because the latter applies over a region of validity extending over several decades in Ca_F it will be taken as the predominant scaling result. The latter result would have been obtained also had we assumed that most of the pressure drop occurs in the displacing nw phase and neglected the pressure drop in the displaced phase. Such an assumption was made by Lenormand [17] in delineating the percolation-to-compact boundary and is also implicit in the analysis of Wilkinson's [9]. Then Eq. (14) becomes

$$\Delta p_F \approx \frac{Ca_F C}{2\Sigma} \sigma^{[\xi + \nu(D-1)]/\nu}, \quad (19)$$

which, in conjunction with Eq. (15), leads to the asymptotic result

$$\sigma \sim \left(\frac{Ca_F C}{2\Sigma} \right)^{-\nu/[1 + \xi + \nu(D-1)]}. \quad (20)$$

Equation (20) expresses the asymptotic scaling of the front (or front-tail) width with Ca_F at small Ca_F for the case of a stabilized displacement.

As in previous studies [9,17,18], the scaling (20) is a power law. In fact, the exponent $\nu/[1 + \xi + \nu(D-1)]$ is *identical* to Wilkinson's $\nu/(1+t-\beta+\nu)$ (substitute ξ in

terms of t and make use of the well-known percolation relation $D = d - \beta/\nu$). This exponent would also have coincided with Lenormand's for the scaling of the percolation-to-compact boundary had we assumed $Q_{nw} = Q$ at the front, which in the present context is tantamount to taking $D = 2$. As shown below, however, Wilkinson's result was obtained differently, by extrapolating in the frontal region the *continuum* solution valid behind the front. The fact that the present work reproduces his result shows that the two approaches are consistent in the case of stabilized displacements.

Using accepted estimates, the exponent in Eq. (20) is equal to 0.382 or 0.25 in two or three dimensions, respectively. The rather small values suggest a weak sensitivity of σ on Ca_F , C , and Σ . It should be kept in mind that the rate dependence in Ca_F has entered through the front velocity v . This can be of some significance in investigating the effect of M , which also influences v [24]. It is also interesting to note that as the degree of heterogeneity Σ increases the front width increases. In fact, Eq. (20) suggests that for such displacements it is more appropriate to replace, in the definition of the capillary number, γ by the product $\gamma\Sigma$. We finally note that the scaling (20) can be also obtained by using a version of GP, termed viscous gradient percolation (VGP), to be introduced below for modeling the saturation profile. Although necessary for the saturation profile, VGP is not required for the derivation or the validity of the scaling (20).

2. Compact region

Sufficiently behind X_c , the previous theory is no longer applicable, as the displacement patterns are compact and fractal notions do not apply. Locally, however, the displacement is still controlled by capillarity, assuming sufficiently low Ca . We proceed by assuming that the injection rates are sufficiently small for gradients in volume-averaged quantities to be small and volume averages to be meaningful. Conditions for the validity of this assumption are developed in a later section. Here we can proceed with the standard continuum description [9,29], in which the individual phase velocities obey an extended Darcy law

$$\mathbf{q}_i = - \frac{kk_{ri}}{\mu_i} \nabla P_i \quad \text{for } i = w, nw \quad (21)$$

and capillary equilibrium applies

$$P_{nw} - P_w = P_c(S_{nw}). \quad (22)$$

The relative permeabilities k_{ri} and the capillary pressure P_c are functions of the saturation S_{nw} , in principle computable from the simulation of an IP process for $p > p_c$. Using OP, Heiba *et al.* [30] and Sahimi [31] evaluated such functions for Bethe and regular lattices, respectively, while Wilkinson [9] has described their asymptotic behavior using IP. In these approaches, the relative permeability functions of the two phases are computed as the relative conductances of two phases ("occupied" and "empty"), randomly distributed following the occupancy patterns of OP (although a more appropriate description should be based on occupancy patterns involving IP with trapping [27]). In either case, the scales are separated and a standard continuum argument can

be used to lead to the following well-known equation for the description of 1D displacements:

$$\phi \frac{\partial S_{nw}}{\partial t} + q \frac{\partial f_{nw}(S_{nw})}{\partial x} = \frac{\partial}{\partial x} \left(\frac{kk_{rw}f_{nw}}{\mu_w} \frac{\partial P_c}{\partial x} \right), \quad (23)$$

where the fractional flow

$$f_{nw} = \left(1 + \frac{k_{rw}\mu_{nw}}{k_{rnw}\mu_w} \right)^{-1} \quad (24)$$

and the capillary pressure $P_c = \gamma J(S_{nw})/\sqrt{k}$ are functions of S_{nw} . For homogeneous systems, we further write

$$\phi \frac{\partial S_{nw}}{\partial t} + q \frac{\partial f_{nw}(S_{nw})}{\partial x} = \frac{\partial}{\partial x} \left(\mathcal{D}(S_{nw}) \frac{\partial S_{nw}}{\partial x} \right), \quad (25)$$

where we introduced the diffusion coefficient $\mathcal{D} = (\gamma\sqrt{k}k_{rw}f_{nw}/\mu_w)(dJ/dS_{nw})$. A direct consequence of the continuum description is that the relevant length scale for saturation changes, hence of the upstream region of the front, is $\sqrt{k} Ca^{-1}$. The difference in the scaling exponents in the two regions suggests a higher sensitivity of the saturation profiles in the compact regime compared to that in the frontal region.

In a region adjacent to the front (termed the "critical region" in [9]), percolation theory can be applied to provide the asymptotic behavior at small S_{nw} of the relative permeability and capillary pressure functions. Based on this behavior and assuming a traveling-wave solution, Wilkinson solved the continuum equation (25) to obtain the local saturation profile around X_0 , which he defined as the "leading edge of the front" and denotes the place where S_{nw} vanishes. In our notation, Wilkinson's result reads

$$S_{nw} \sim \left(\frac{Ca_F C}{\Sigma} (X_0 - X) \right)^{\beta/(1+t-\beta)}, \quad (26)$$

where we also included the heterogeneity factor Σ . Using the percolation result $S_{nw} \sim \Delta p^\beta$, one further obtains the profile of the percolation probability in this region

$$\Delta p \sim \left(\frac{Ca_F C}{\Sigma} (X_0 - X) \right)^{1/(1+t-\beta)}. \quad (27)$$

It should be remarked that if we adopt the above definition for X_0 , it must follow that $X_0 > X_c$ (in fact, $X_0 \approx X_c + \sigma$). But then Eqs. (26) and (27) would not be strictly valid, as the region of integration would also include the front-tail region ($X_c < X < X_0$), where the above continuum equations do not apply. Thus it is more appropriate to take $X_0 \equiv X_c$ instead and to accept the validity of these equations only in the critical region (where $X < X_c$). This is equivalent to shifting the traveling front by a constant and will be considered below in modeling the saturation profile. In their present form, Eqs. (26) and (27) must be viewed as an approximate composite solution that spans both the fractal and the compact regions and approaches asymptotically, in the far field, the continuum scaling (26).

Equation (27) was used by Wilkinson [9] to obtain an estimate of the front-tail width by proceeding essentially as

follows. Evaluating Eq. (27) at $X=X_c$, taking $\sigma_c=X_0-X_c$, and using subscript C to denote the critical region gives

$$\Delta p_C \approx \left(\frac{\text{Ca}_F C \sigma_C}{\Sigma} \right)^{1/(1+t-\beta)}, \quad (28)$$

which is the counterpart of our Eq. (19). Both equations are power laws, but with different exponents. In fact, the exponent of Eq. (19) is always greater than one, whereas that of Eq. (28) is always smaller than one. Moreover, the dependence of Δp (hence of ΔP_C) on Ca_F is different in the two cases (linear vs nonlinear). Next, the previous GP argument is applied by using Eq. (15) in Eq. (28) to obtain the scaling of σ_C with Ca_F . We find the result

$$\sigma_C \approx \left(\frac{\text{Ca}_F C}{\Sigma} \right)^{-\nu/(1+t-\beta+\nu)}, \quad (29)$$

which, in view of the relation between t and ζ , is *identical* to our Eq. (20). The coincidence of the two exponents is rather remarkable, given that one approach uses scaling laws in a fractal region, while the other is based on a continuum description (the solution of a differential equation, although a GP self-consistency argument was also used), while at the same time the various profiles are markedly different in the two cases. The reason for this coincidence is that in both cases the front width σ also happens to be the length of the interval ξ , where the overall capillary pressure difference ΔP_c is the same for both approaches. Indeed, if we equate the corresponding two expressions for ΔP_c (or, equivalently, Δp) over an increment ξ , we have

$$\text{Ca}_F \xi^{(t-\beta+\nu)/\nu} \sim (\text{Ca}_F \xi)^{1/(t-\beta+1)}, \quad (30)$$

the solution of which is $\xi \sim \text{Ca}_F^{-\omega}$, where ω is the previous exponent $\omega = \nu/(1+t-\beta+\nu)$; hence we have $\xi \sim \sigma \sim \sigma_C$.

3. Saturation profile

Equation (20) provides the scaling of the front width with Ca_F . The other important quantity in gradient percolation is the saturation profile. Gouyet, Sapoval, and Rosso [6] and Hulin *et al.* [13] discussed scaling properties of saturation profiles for the classical GP and IPG problems, where the percolation probability increment across a region scales linearly with its extent. In the case of a constant gradient, the scaling of the profile is given by [6]

$$S_{nw} \sim p B^{\beta/(1+\nu)} \Pi_f \left(\frac{X_c - X}{\sigma} \right), \quad (31)$$

where $\Pi_f(u)$ is a scaling function that approaches the ordinary percolation scaling, $\Pi_f(u) \sim u^\beta$, when $u > 0$, and it is approximately described by the best-fit expression

$$\log_{10} \Pi_f(u) = -1.1u^2 + 0.48u + 0.10, \quad (32)$$

when $u < 0$. For the case of viscous displacement, we first need to find the variation of Δp across an arbitrary (but suitably constrained) increment χ within the fractal region ($\chi < \sigma$). This problem is equivalent to determining the variation of the transversely averaged pressure within a percola-

tion cluster, across which a fixed pressure difference is applied. It can be deduced that this profile is linear; thus we have

$$\Delta p = \frac{\chi \Delta p_F}{\sigma} \quad (33)$$

and therefore

$$\Delta p \approx \frac{\text{Ca}_F C}{2\Sigma} \chi (\sigma^{[\zeta + \nu(D-2)]/\nu} - bM) \quad (34)$$

for the variation of p across such an increment. The variation in Eq. (34) is linear with respect to χ .

An approximate description of the saturation profile can now be obtained by using a model GP in which the percolation probability has the profile suggested by Eq. (27) and (34) on the respective sides of X_c . The resulting composite profile of p is shown in Fig. 5. The percolation probability gradient at p_c is constant, as we approach X_c from the right, but diverges as we approach it from the left. This feature is different from the classical IPG, where the gradient at p_c is constant. In actuality, the dependence of the profile near p_c is not as extreme as indicated and a more appropriate profile should involve a composite curve that only asymptotically approaches in the far field the respective limits. The particular profile depicted in Fig. 5 gives rise to a different GP problem, to be termed viscous gradient percolation.

Viscous gradient percolation. We consider a static percolation problem in a lattice with a percolation probability gradient that is constant at the percolation threshold from the right and diverges from the left, namely,

$$p - p_c = \begin{cases} -B^a(X - X_c) & \text{for } X > X_c \\ [B(X_c - X)]^c & \text{for } X_c \geq X. \end{cases} \quad (35)$$

Here $B > 0$ denotes an equivalent Bond number, exponents $a > 0$ and $0 < c < 1$ are arbitrary, and capital letters denote distances in lattice units. In the specific problem under consideration, we have $a = (1 + \nu)/[1 + \zeta + \nu(D - 1)]$ and $c = 1/[1 + \zeta + \nu(D - 2)]$. We conducted numerical simulations for this gradient percolation problem for values of a and c corresponding to three dimensions. Figure 5 shows probability and saturation (transversely averaged occupancy) profiles plotted vs normalized distance for two different values of B . The overall features of the saturation profiles are similar to GP: The profile decreases almost linearly with distance in the region upstream of the front and the front extent increases as B decreases. (The different lattice sizes used in the normalized plots of these figures should be noted.) The scaling of the saturation profile is expected to have the general features of the scaling function (31) of the standard GP, with some correction to account for the slightly different VGP profile.

By applying the self-consistency argument of GP, a power-law scaling for the front width with B can be obtained. Indeed, using the percolation scaling $p_c - p \sim \sigma^{-1/\nu}$ and substituting $X - X_c \sim \sigma$ in the top member of Eq. (35) leads to the power-law scaling

$$\sigma \sim B^{-a\nu/(1+\nu)}. \quad (36)$$

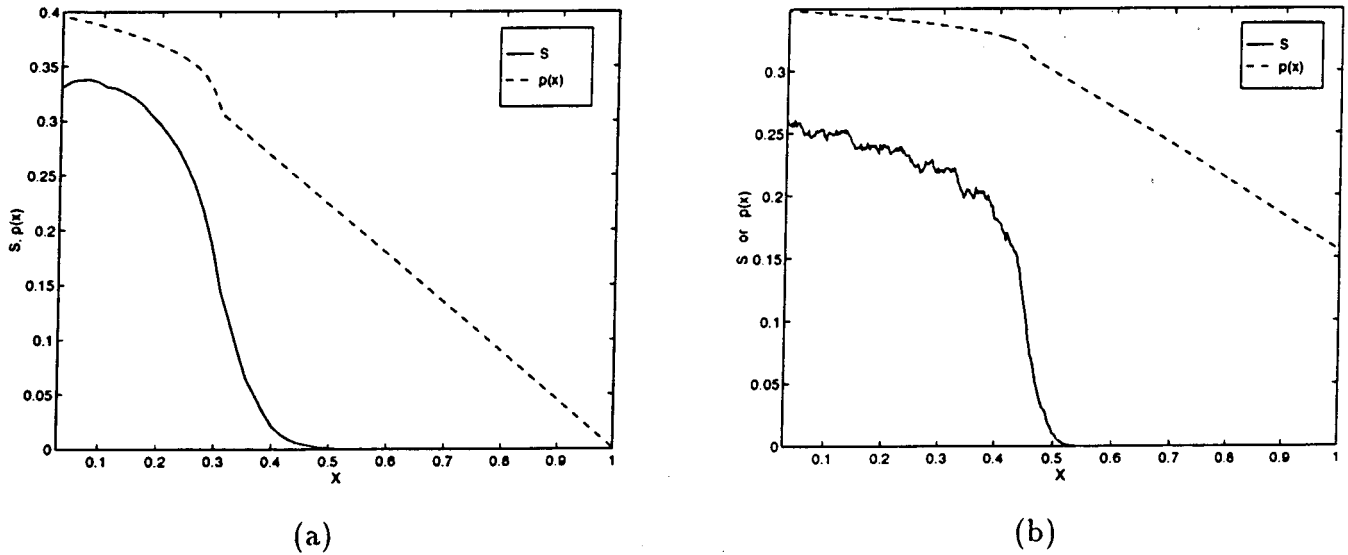


FIG. 5. Percolation probability (dashed line) and saturation (solid line) profiles vs normalized length, for 3D VGP: (a) $B = 10^{-4}$ in a lattice of $200 \times 200 \times 65$ and (b) $B = 10^{-6}$ in a lattice of $200 \times 200 \times 500$.

Since in this limit $B^a = (\text{Ca}_F C / 2\Sigma) \sigma^{[\zeta + \nu(D-2)]/\nu}$, Eq. (36) leads to the same scaling as Eq. (20). An *identical* power law would have also been obtained had we used the lower member of Eq. (35), namely, had we extended the definition of σ upstream of X_c and made use of the scaling (15) in the regime upstream of X_c . Essentially, this was the approach taken by Wilkinson [9]. Again, this coincidence is due to the specific relation between a and c and has the same interpretation given above.

We summarize this section by emphasizing the different description of percolation processes involving viscous forces in the two regions, near and away from the front, at least for relatively low Ca . The different scalings $\text{Ca}_F^{-\nu/[1+\zeta+\nu(D-1)]}$ and Ca^{-1} obtained indicate that near the front, the continuum description (25) for the profile should be replaced with the more appropriate VGP equation (31). Either theory suggests an advancing front. In the VGP model, the profile is a function of $X - X_c$, Ca_F , and M , the time dependence entering through X_c , which varies with time. A traveling state with constant velocity is also contained in the continuum description (25). However, the latter predicts a *hypodiffusive* behavior [29], namely, a profile with a divergent derivative at the front (a sharp ‘‘knee’’), in contrast to the tail involved in VGP. Thus appropriate caution must be exercised in using the continuum approach in this region.

4. Region of validity of stabilized displacements

The above scaling was obtained under the assumption that the fully developed displacement is stabilized. This requires that the percolation probability decreases in the direction of displacement for all increments $\chi < \sigma$, namely, that the right-hand sides of Eqs. (12) and (14) are positive. However, in the preceding section it was shown that provided that the displacement is stabilized, a solution for σ always exists and thus the right-hand sides of Eqs. (12) and (14) are always positive. Therefore, in order to establish a condition for the existence of a stabilized displacement, we must address the *initial* phase of the displacement, before a saturation profile

or a traveling-wave solution develops. This problem is a variation of the problem treated by Lenormand [17].

Consider, then, the pattern at the onset of displacement, which will be assumed to be of the percolation type and of an extent $\chi \times L^{d-1}$, where χ is an increasing function of time, until a saturation profile starts developing. The latter will occur at $\chi < \chi_e$, where $\chi_e(\text{Ca}, M)$ is the limiting size, above which the displacement ceases to be a percolation process. Lenormand has determined χ_e in two limiting cases, where pressure drops occur only in one of the two phases, respectively. For the solution of the present problem, the more general case needs to be considered. Because of the considerable details involved, the results are presented in a separate study [23]. Here we simply note that the difference in capillary pressure can be evaluated as before, except that now $Q_{nw} = Q$, since a traveling-wave solution or a fully developed displacement has not yet developed (this was also taken by Lenormand [17]). Assuming that percolation scalings apply, the capillary pressure drop over this region of size $\chi \times L^{d-1}$ at the entrance of the displacement reads

$$\Delta P_c = \frac{Aq\mu_{nw}}{r_m} \chi (\chi^{[\zeta + \nu(D-2)]/\nu} - eM), \quad (37)$$

where e is another $O(1)$ constant. It is apparent that for the formation of a stabilized displacement, the right-hand side of Eq. (37) must be positive for all $\chi < \chi_e$. Clearly, this requires that M be sufficiently small. This condition is implied in Lenormand’s [17] description of the validity of the percolation regime, which indicates a transition around $M \sim 1$. It is shown in [23] that the displacement is *unconditionally* stabilized if $M < M^*$, where $M^* \approx 1$, and *conditionally* stabilized in the opposite case. In the latter, stabilized displacement is still possible, however, provided

$$\frac{\text{Ca}}{\Sigma} M^{[\zeta + 1 + \nu(D-1)]/[\zeta + \nu(D-2)]} \ll 1 \quad (38)$$

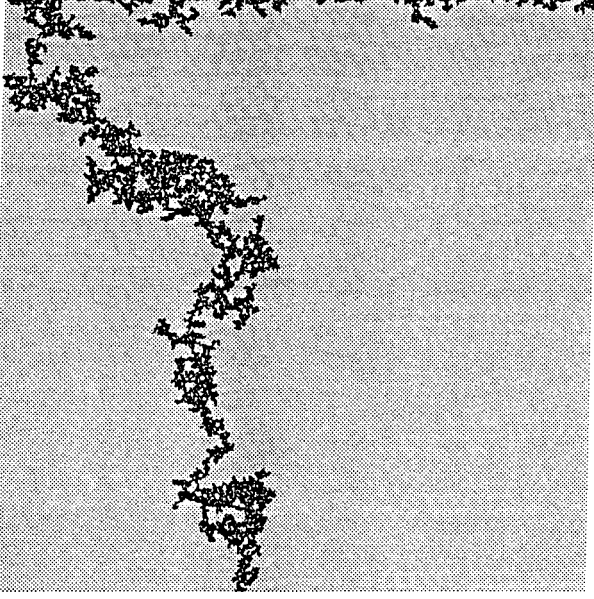


FIG. 6. Single finger in GP in a destabilizing gradient (from [8]).

(see [23] for details). Equation (38) shows that the displacement is stabilized even if M is large, provided the capillary number is sufficiently small. In such a case, a stabilized displacement would develop for values of M larger than $M = 1$. This supports the validity of the Buckley-Leverett description for a wide range of parameter values, as commonly practiced in applications.

B. Capillary-viscous fingering

When condition (38) is violated, for example, when the nw fluid has a much smaller viscosity, most of the pressure drop occurs within the displaced phase. In such cases p increases in the direction of displacement. IPG problems with spatially increasing percolation probability involve a negative Bond number and describe invasion in a destabilizing gradient [14,15]. In particular, capillary invasion in a destabilizing gravity field, for example, corresponding to the release of a lighter fluid at the bottom of a porous column filled with a heavier fluid, was studied in considerable detail [15] (see also the related problems of [8,16]). It was found that the displacement occurs in the form of distinct capillary (but not DLA-type) fingers. For a sufficiently long column, one single finger emerged. Figure 6, reprinted from [8], shows the structure of such a finger for capillary invasion in a field of increasing permeability. Scaling arguments similar to the self-consistency arguments of GP can be used here [9,15] to show that the finger consists of a string of beads of average width σ with the scaling behavior.

$$\sigma \sim |B|^{-\nu/(\nu+1)}. \quad (39)$$

To apply these findings to the viscous problems of interest here, an expression for B is needed.

Consider ΔP_c (and Δp) across an element of size σ^d in the geometry of Fig. 6. In contrast to the stabilized displacement, where it spans the entire cross section of the sample of

area $\sim L^{d-1}$, here the nw phase occupies narrow fingers. Thus the appropriate expression corresponding to Eq. (7) is

$$\Delta P_{nw} = \frac{A Q_{nw} \mu_{nw}}{r_m^3} \sigma^{\xi/\nu}, \quad (40)$$

where $Q_{nw} = Q = qL^{d-1}l^2$. The equation for the pressure drop of the w phase remains the same as Eq. (11). After some manipulations we obtain the equation for the variation of p across an increment of size σ ,

$$\Delta p \approx \frac{A Ca l^2}{2 \Sigma r_m^2} \sigma \left(\frac{L^{d-1} \sigma^{(\xi-\nu)/\nu}}{n} - b' M \right), \quad (41)$$

where $b' = Er_m/Al$ is another $O(1)$ constant and n is the number of fingers that develop. Now, if we further assume that the last term in large parentheses on the right-hand side of Eq. (41) is the dominant term, we can identify a suitable bond number for this problem, namely,

$$B = - \frac{E Ca M l}{2 \Sigma r_m} \approx - \frac{E Ca M}{2 \Sigma}. \quad (42)$$

This assumption is equivalent to neglecting the pressure drop in the displacing phase (as also done by Lenormand [17]). Using this definition, a direct comparison with Eq. (39) gives the result for the finger width

$$\sigma \sim \left(\frac{E Ca M}{2 \Sigma} \right)^{-\nu/(\nu+1)}. \quad (43)$$

In the more general case where the second term on the right-hand side of Eq. (41) is not necessarily dominant, the dependence of σ on the parameters is different and would be obtained by solving the equation

$$\frac{A Ca l^2}{2 \Sigma r_m^2} \sigma \left(\frac{L^{d-1} \sigma^{(\xi-\nu)/\nu}}{n} - b' M \right) \sim - \sigma^{-1/\nu}. \quad (44)$$

The power law of Eq. (43) has the familiar GP exponent, with values 0.571 or 0.469 in the respective geometries (compared to 0.382 or 0.25 of the previous case). This exponent is identical to Lenormand's [17] for the scaling of the percolation-to-viscous fingering boundary (arrow CD in Fig. 1), although his exponent did not pertain to the width of a finger or to the particular regime of destabilizing GP discussed here. (However, it was pointed out that the transition would eventually result in fingers continuously thinning as the DLA regime is approached.) A comparison with Eq. (20) shows that the scaling exponent almost doubles as the mobility ratio increases from the one limiting regime to the other, implying a higher sensitivity on the capillary number. Equation (43) also shows that the finger width decreases with an increase in the capillary number Ca and the mobility ratio M and that it eventually reduces to a single thin finger of the size of a single pore (and where the above scaling fails and a DLA regime emerges). This behavior is as expected.

We also note that Eq. (43) can be approximated rather well (at least in three dimensions) with the expression

$$\sigma \sim Ca^{-0.5}. \quad (45)$$

This scaling is consistent with that of the fastest (most dangerous) growing finger predicted by the linear stability analysis of Chuoke, van Meurs, and van der Poel [21,32], which suggests an exponent equal to $\frac{1}{2}$. However, the two should not be confused. The present analysis is based on finger widths of the order of the pore scale, while the linear stability analysis of [21] is actually based on a continuum description of stabilized displacements, using an *ad hoc* expression for the interfacial behavior in the form of an effective macroscopic interface.

A necessary condition for the validity of Eq. (43) is $\Delta p < 0$ in Eq. (41). This is automatically satisfied, provided Eq. (44) has a solution. This equation can be rearranged to read

$$b'M \approx \frac{L^{d-1} \sigma^{(\zeta-\nu)/\nu}}{n} + \frac{F \Sigma \sigma^{-1/\nu}}{\text{Ca}}, \quad (46)$$

where F is a positive constant. Contrary to the previous problem of stabilized displacement, however, it can be shown that a solution of the above *does not* exist for an arbitrary value of M (at least under the condition that the finger spacing remains constant). Indeed, the right-hand side $G(\sigma)$ of Eq. (46) goes through a minimum at the value $\sigma^* \sim (n/L^{d-1}\text{Ca})^{\nu/(\zeta+1)}$, where $G(\sigma^*) \sim (L^{d-1}/n)^{(\nu+1)/(\zeta+1)} \text{Ca}^{-(\zeta-\nu)/(\zeta+1)}$. Thus a condition for the existence of the fingering regime is that a solution exists, namely, that

$$M > \left(\frac{\zeta+1}{\zeta-\nu} \right) \left(\frac{\nu+1}{\zeta-\nu} \right)^{-(\nu+1)/(\zeta+1)} \left(\frac{L^{d-1}}{n} \right)^{(\nu+1)/(\zeta+1)} \times \left(\frac{\text{Ca}}{F \Sigma} \right)^{-(\zeta-\nu)/(\zeta+1)}. \quad (47)$$

Based on Eq. (47) we can make the following remarks: (i) For fixed finger spacing L^{d-1}/n , this fingering regime is reached at smaller values of M as Ca/Σ increases (although one should note that the exponent of Ca is rather small and equals 0.11); this is as expected. However, (ii) the spacing between the fingers L^{d-1}/n enters explicitly in the above condition, thus the utility of Eq. (47) is unclear at present. One could advance the argument that Eq. (47) actually defines the finger spacing, namely, that

$$\frac{L^{d-1}}{n} \sim M^{(\zeta+1)/(\nu+1)} \text{Ca}^{(\zeta-\nu)/(\nu+1)}. \quad (48)$$

Such a conjecture would mean that the percolation probability always remains near p_c , an idea consistent with self-organized criticality arguments, and would indicate a decrease in the number of fingers with an increase in M and or Ca . Additional work is needed to test this hypothesis, however.

The above analyses show that the displacement behavior is different depending on the relative magnitude of M . This is a direct consequence of the pressure drop in the frontal region in the two cases of low or high M , respectively. In either case, the pressure drop is associated with the higher flow resistance. In the first case, it is due to the invading phase, which near the front occupies a percolationlike cluster. In the second case, it is due to the displaced phase, which

near the front occupies a compact region. The different behavior in these two limits is the origin of the difference in the scaling exponents in the two limits. Such a distinction was made by Lenormand [17], but not by Wilkinson [9] or Blunt, King, and Sher [18]. This explains why our exponent agrees with Wilkinson's only in the first case, but not in the second, where instead we agree with Lenormand. The difference between our exponent and Lenormand's [17] for the case of low M is due to the fact that Lenormand [17] used the entire injection rate Q , while here we assumed that only a small fraction of Q actually reaches the frontal region. This difference is ultimately reflected in the scaling exponents. We must point out, however, that Lenormand's assumption is correct for the specific problem he considered, which is the evaluation of the departure from percolation in a displacement in a square lattice, where traveling fronts and gradient percolation concepts are not involved.

III. EXPERIMENTS

The VGP theory at small M was partially tested by conducting some experiments and pore-network simulations. Immiscible displacement experiments were conducted in a long sample, consisting of a vertically placed rectangular glass bead pack of dimensions $30 \times 4 \times 2 \text{ cm}^3$, filled with $100\text{-}\mu\text{m}$ glass beads, with porosity and permeability equal to $\sim 40\%$ and $\sim 40 \times 10^{-12} \text{ m}^2$, respectively. Gravitational effects were avoided by using matched-density fluids ($\rho = 1.15 \times 10^3 \text{ kg m}^{-3}$, $\delta\rho < 10 \text{ kg m}^{-3}$). A water-sucrose mixture was used as the wetting fluid ($\mu_w = 5 \times 10^{-3} \text{ Pa s}$) and dibutyl phthalate was used as the nonwetting fluid ($\mu_0 = 14 \times 10^{-3} \text{ Pa s}$), resulting in a viscosity ratio of $M = 0.3$. The interfacial tension between the fluids was $\gamma \sim 25 \times 10^{-3} \text{ J m}^{-2}$.

Experiments corresponded to primary drainage and involved the displacement of the wetting fluid from an initially water-sucrose-saturated sample by the nonwetting fluid. The flow rate q varied between 10^{-6} and 10^{-4} m/s , corresponding to a capillary number variation in the interval between 5×10^{-7} and 5×10^{-5} . An acoustic technique, described elsewhere [33], was used to determine the saturation profile. Saturation measurements were indirectly obtained from the velocity variations of a sound wave along the sample. From the calibration curve [33] and the accuracy of the relative velocity measurements (10^{-4}) we estimate the overall accuracy in saturation as better than 1%. A spatial resolution of 1 mm was implemented in order to keep track of precise variations along the length of the sample.

Figure 7 shows a log-log plot of the front extent vs capillary number obtained experimentally. The extent of the front was obtained by using the scaling function of GP as detailed in [8]. The data show that the relationship is a straight line, although there is some scatter. The data can be fitted quite well with a straight line of slope of -0.25 in good agreement with the theoretical prediction. Even though the agreement is good, additional experiments would be needed for a more rigorous test of the theory.

The predictions for the small M case were also tested with results from 2D pore-network simulations using the drainage network model described by Xu [25]. Simulations in a 40×100 network, with $M = 0.1$ and Ca varying in the interval

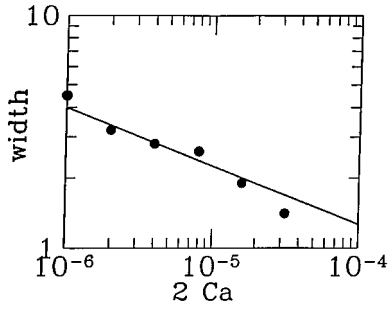


FIG. 7. Plot of the front width vs Ca from experimental results. The solid line is the theoretical prediction of slope -0.254 . The front width is dimensionless using the bead size as the characteristic size.

between 10^{-4} and 10^{-5} , showed a power-law scaling of the front width with the capillary number, with a best-fit slope of -0.34 (Fig. 8), in reasonable agreement with the expected value -0.382 . Given the various finite-size effects due to the small sizes of the network, this agreement is somewhat surprising. A more stringent test should involve much larger lattices and much smaller Ca . Work in this direction is also currently under way. Additional work is also needed to explore the fingering regime and to test the constraints (38) and (47) and the conjecture (48).

IV. REMARKS ON THE EFFECT OF HETEROGENEITY

We conclude this paper by making additional remarks on the validity of the continuum theory. The latter was based on the assumption that expressions such as Eq. (21), are deterministic, namely, that saturation gradients are sufficiently small for volume-averaged quantities to be statistically meaningful. To set a quantitative condition for the validity of this assumption we proceed as follows.

Consider a 3D volume containing N_s occupied and uncorrelated pores with the statistics described before and define a volume-averaged quantity $\langle \Psi \rangle_{N_s}$ over this volume. In gen-

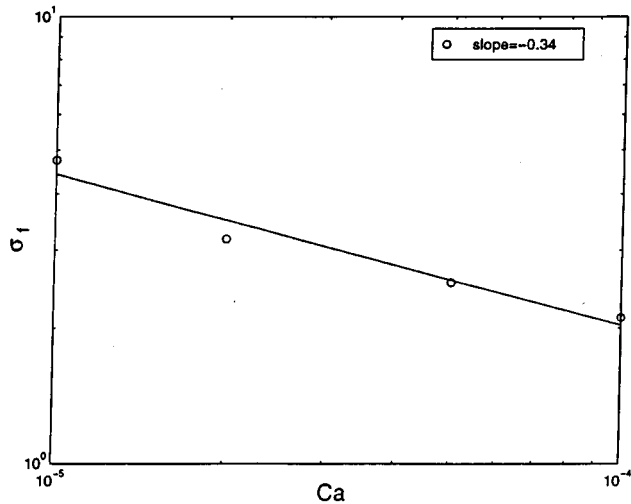


FIG. 8. Plot of the front width vs Ca from pore-network simulations with $M=0.1$ in a lattice of 60×100 . The best-fit slope of -0.34 compares reasonably well with the theoretical prediction of -0.384 .

eral, this quantity is a random variable with a deterministic mean and a standard deviation that, in the large- N_s limit, scales as $\Sigma N_s^{-1/2}$, as dictated by the law of large numbers [34]. This property is shared by all volume-averaged quantities, such as pressure and permeability. The conventional continuum description above relies on the existence of deterministic volume averages and hence on the requirement that the standard deviation of the volume averages does not exceed a small positive number δ , namely, that

$$N_s \geq \left(\frac{\Sigma}{\delta} \right)^2. \quad (49)$$

Condition (49) shows that, as expected, more disordered media require a larger averaging volume for the definition of meaningful averages. For quantities that depend on the saturation (such as relative permeabilities and capillary pressures), however, deterministic volume averages additionally require that saturations are spatially uniform, namely, that the scaled saturation gradient in the volume-averaged region $g = -dS_{nw}/dX$ is sufficiently small,

$$g \leq \frac{\epsilon}{N_s^{1/3}}, \quad (50)$$

where ϵ is the allowed standard deviation of S_{nw} (e.g., of the order of 10^{-3}). In the continuum description above, g was shown to scale with Ca . The two inequalities can be combined to lead to the condition for the validity of the continuum description

$$Ca \leq O \left(\epsilon \left(\frac{\delta}{\Sigma} \right)^{2/3} \right). \quad (51)$$

Typical displacements are usually conducted at $Ca=10^{-6}$, which appears to be within the range defined by Eq. (51). However, it becomes more difficult for this condition to be satisfied as the disorder Σ increases.

The previous theory identified three length scales of relevance to drainage processes in uncorrelated random media: In dimensionless terms, they are proportional to L (the lateral extent), to $Ca_F^{-\nu/[1+\zeta+\nu(D-1)]}$ (case 1) or $Ca^{-\nu/(1+\nu)}$ (case 2), and to Ca^{-1} . Heterogeneity in the pore structure can enter either through gradients in the mean pore size (in which case the pore size becomes a nonstationary variable) or through stationary, but spatially correlated, pore sizes. In either case, its effect on the saturation profile depends on the magnitude of the appropriate length scale. In the case of pore size gradients, the heterogeneity Bond number [8] $B_k = -dr_m/dx$ introduces a corresponding length scale that is proportional to B_k^{-1} . Here effects of heterogeneity can still be captured by continuum equations provided the relevant length scales discussed above are smaller than this scale, which would then impose upper bounds on Ca . In addition, use of volume-averaged quantities requires sufficiently weak heterogeneity, namely,

$$B_k < \delta^{2/3}. \quad (52)$$

Otherwise, heterogeneity would interfere with the development of the saturation profile. This can still be handled with the previous approach, however. For example, in the absence

of viscous forces it is known that gradients in the mean pore size lead to a stable form of IPG when $B_k > 0$ and to an unstable form of IPG (capillary fingering) in the opposite case [8]. Thus, when viscous forces are also considered, we can combine heterogeneity and viscous gradients in an *additive* operation, the resulting scaling with respect to Ca now being accordingly different.

Different considerations apply when the local pore size is stationary but spatially correlated, with a dimensionless correlation length λ . Here the previous theory is still applicable, provided the corresponding viscous lengths exceed λ significantly. Otherwise, the displacement would be affected by the heterogeneity. Recent work [35] has studied effects of spatial correlations (involving fractal statistics) on IP.

When, as result of increased Ca, conditions such as Eq. (51) are violated, many of the previous postulates, for example, the concept of deterministic volume averages, become questionable. In this case, suitable alternatives to the above must be sought. One approach could involve defining area (instead of volume) averages, transverse to the main direction of displacement, provided the lateral extent is sufficiently large. Here some form of IPG is also expected to be applicable since the displacement remains a percolation process, but with a gradient in the percolation probability. Work in this direction is currently in progress.

V. CONCLUSIONS

In this paper the effect of viscous forces on drainage displacements in porous media was studied. We recognized that

the process, at least near the front, shares common aspects with IPG. When M is sufficiently small, the displacement can be modeled by a form of gradient percolation in a *stabilizing* gradient. We developed the scaling of the front width and the saturation profile, in terms of the capillary number. As the stabilized regime is described by the Buckley-Leverett equation, the two share the same constraints for their validity. In the opposite case, the displacement is described by gradient percolation in a *destabilizing* gradient and leads to fingering. The particular regime involves a competition between capillary and viscous forces. Limited experimental and numerical results support the theory. The effect of heterogeneity was also discussed and upper bound conditions on Ca for the validity of the continuum approach were developed. The theory shows that the conventional continuum approach should be used with caution near the front. Similar results are also expected for imbibition (displacement of a nonwetting phase) provided that injection rates are sufficiently high [36].

ACKNOWLEDGMENTS

The research of B.X. and Y.C.Y. was partly supported by DOE Contract No. DE-FG22-96BC1994/SUB. The collaboration between the authors was facilitated by NATO Grant No. CRG 901053. All these sources of support are gratefully acknowledged. The Laboratoire Fluides, Automatique et Systèmes Thermiques is associated with CNRS (URA 371), Université Paris VI, and Université Paris XI.

-
- [1] R. Lenormand and S. Bories, C. R. Acad. Sci. Paris B **291**, 279 (1990).
- [2] R. Chandler, J. Koplik, K. Lerman, and J. F. Willemsen, J. Fluid Mech. **119**, 244 (1982).
- [3] D. Wilkinson and J. F. Willemsen, J. Phys. A **16**, 3365 (1983).
- [4] J. Feder, *Fractals* (Plenum, New York, 1988).
- [5] D. Wilkinson, Phys. Rev. A **30**, 520 (1984).
- [6] J.-F. Gouyet, B. Sapoval, and M. Rosso, Phys. Rev. B **37**, 1832 (1988).
- [7] A. Birovljev, L. Furuberg, J. Feder, T. Jøssang, K. J. Maloy, and A. Aharony, Phys. Rev. Lett. **67**, 584 (1991).
- [8] M. Chaouche, N. Rakotomalala, D. Salin, B. Xu, and Y. C. Yortsos, Phys. Rev. E **49**, 4133 (1994).
- [9] D. Wilkinson, Phys. Rev. A **34**, 1380 (1986).
- [10] D. Stauffer and A. Aharony, *Introduction to Percolation Theory* (Taylor & Francis, London, 1992).
- [11] M. B. Isichenko, Rev. Mod. Phys. **64**, 961 (1992).
- [12] B. Sapoval, M. Rosso, and J.-F. Gouyet, J. Phys. (France) Lett. **46**, L149 (1985).
- [13] J.-P. Hulin, E. Clément, C. Baudet, J.-F. Gouyet, and M. Rosso, Phys. Rev. Lett. **61**, 333 (1988).
- [14] V. Frette, J. Feder, T. Jøssang, and P. Meakin, Phys. Rev. Lett. **68**, 3164 (1992).
- [15] P. Meakin, J. Feder, V. Frette, and T. Jøssang, Phys. Rev. A **46**, 3357 (1992).
- [16] Y. Deng, I. Chatzis, and F. A. L. Dullien (unpublished).
- [17] R. Lenormand, Proc. R. Soc. London, Ser. A **423**, 159 (1989).
- [18] M. Blunt, M. J. King, and H. Sher, Phys. Rev. A **46**, 7680 (1992).
- [19] L. W. Lake, *Enhanced Oil Recovery* (Prentice-Hall, Englewood Cliffs, NJ, 1989).
- [20] *Reservoir Characterization*, edited by L. W. Lake and H. B. Carroll Jr. (Academic, Orlando, 1986).
- [21] R. L. Chuoke, P. van Meurs, and L. B. van der Poel, Trans. AIME **216**, 188 (1959).
- [22] Y. C. Yortsos and F. J. Hickernell, SIAM (Soc. Ind. Appl. Math.) J. Appl. Math. **49**, 730 (1989).
- [23] Y. C. Yortsos, B. Xu, and D. Salin, Phys. Rev. Lett. (to be published).
- [24] E. D. Chikhliwala, A. B. Huang, and Y. C. Yortsos, Transp. Porous Media **3**, 257 (1988).
- [25] B. Xu, Ph.D. dissertation, University of Southern California, 1995 (unpublished).
- [26] M. Haghghi, B. Xu, and Y. C. Yortsos, J. Colloid Interface Sci. **166**, 168 (1994).
- [27] M. M. Dias and D. J. Wilkinson, J. Phys. A **19**, 3131 (1986).
- [28] A. J. Katz and A. H. Thompson, Phys. Rev. B **34**, 8179 (1986).
- [29] P. G. de Gennes, Physicochem. Hydrodynam. **4**, 175 (1983).
- [30] A. A. Heiba, M. Sahimi, L. E. Scriven, and H. T. Davis, Soc. Pet. Eng. Reservoir Eng. **7** (1992).

- [31] M. Sahimi, Chem. Eng. Commun. **64**, 179 (1988).
- [32] G. M. Homsy, Annu. Rev. Fluid Mech. **19**, 271 (1987).
- [33] J.-C. Bacri and D. Salin, Geophys. Res. Lett. **13**, 326 (1986).
- [34] W. L. Hays and R. L. Winkler, *Statistics: Probability, Inference, and Decision* (Holt, Rinehart and Winston, New York, 1970), Vol. 1.
- [35] C. Du, C. Satik and Y. C. Yortsos, AIChE. J. **42**, 2392 (1996).
- [36] R. Lenormand, J. Phys.: Condens. Matter **2**, SA79 (1990).